Gold Bull (2016) 49:95–102
DOI 10.1007/s13404-016-0187-3

ORIGINAL PAPER

Green electrodeposition of gold nanostructures by diverse size, shape, and electrochemical activity

R. Dehdari Vais[1] · **N. Sattarahmady**[1,2] · **H. Heli**[1]

Received: 18 April 2016 / Accepted: 24 October 2016 / Published online: 9 November 2016

Abstract Variety of shapes of gold nanostructures with different sizes from zero-dimensional nanoparticles to hierarchical structures were prepared by one-step template-less green electrodeposition methods. Additives added to the synthesis solution played a vital role to determine the morphology of the nanostructures. The nanostructures represented different electrochemical activities toward the redox processes of some biologically important compounds attributing to the size and shape of the nanostructures.

Keywords Nanoparticle · Gold · Electrodeposition · Green synthesis

Introduction

Nanostructured noble metals with diverse size, shape, morphology, and crystal orientation have attracted much attention due to a porous nature, high and favorable surface areas, and unique physical and chemical properties different from their bulk counterparts [1]. In this regard, noble metal nanorods [2], nanowires [3], nanoflowers [4], nanorings [5], nanobelts [6], nanocubes [7], nanoprisms [8], and nanoplates [9] were synthesized. These nanostructures have potential applications due to special electronic, optical, thermal, catalytic, or magnetic functions [1, 10]. Among the noble metals, gold nanostructures are of importance due to their unique physicochemical properties arising from size and collective effects [11], shape [1, 12], atomic arrangement [13], electronic properties [14], and the local dielectric property [15]. Therefore, the precise control of size and shape is the key parameter to better understand and control the physicochemical properties of gold nanostructures [16]. Gold nanostructures have extensive applications in catalysis and electrocatalysis [17], sensing and biosensing [18], electronic and optical detecting systems [19], surface-enhanced Raman spectroscopy [20], chemical analysis [21], fuel cells [22], photothermal therapy [23], antibacterial nanomedicine [24], and radiotherapy [25].

Up to now, different methods have been developed for the synthesis of gold nanostructures including simple chemical reduction, seed mediation, photoreduction, sonochemical, template-based method, solvothermal, hydrothermal, electrodeposition, galvanic replacement, layer-by-layer self-assembly, selectively de-alloying, and lithography [17, 26]. Using these methods, various sizes and shapes of zero-to-three-dimensional gold nanostructures including nanoparticles [27, 28], hollow nanotubes [29], nanorods [30], nanoflowers [31], nanodendrites [32], hollow spheres [33], anisotropic nanoparticles and plates [34], nanopyramidal, nanorod-like, and spherical nanostructures [35, 36], nanoblooms [37], nanospears [38], nanoleaves and nanoleaflets [39, 40], nanostars [41], porous textile-like sheet arrays [42], nanodumbbells, nanopods, and nanodendrites [26] were synthesized.

Electrodeposition synthesis of nanostructured materials (including gold nanostructures) is a potentially superior method due to advantages of having a high degree of controllability, being single-step process and easy control, having

Electronic supplementary material The online version of this article (doi:10.1007/s13404-016-0187-3) contains supplementary material, which is available to authorized users.

✉ H. Heli
hheli7@yahoo.com; heli@sums.ac.ir

[1] Nanomedicine and Nanobiology Research Center, Shiraz University of Medical Sciences, Shiraz, Iran

[2] Department of Medical Physics, School of Medicine, Shiraz University of Medical Sciences, Shiraz, Iran

effective controllable of size and shape of the electrodeposits, being easy to anchor securely on the substrate, producing uniform and high pure deposits, being environmentally friend, and providing more opportunities for the design and fabrication of different devices [26–32, 35–40, 43].

In the present study, one-step, green, and template-less electrodeposition methods were developed to fabricate gold nanostructures with different sizes and shapes.

Experimental section

Reagents and chemicals

All chemicals were of analytical grade form Merck (Germany) or Sigma (USA) and were used without further purification. All solutions were prepared with doubly distilled water.

Apparatus

Electrochemical experiments were carried out in a conventional three-electrode cell containing a supporting electrolyte (including synthesis solutions or else) powered by a μ-Autolab type III potentiostat/galvanostat (The Netherlands). An Ag/AgCl, saturated KCl, a glassy carbon rod, and a gold disk (Au) electrode were used as the reference, counter, and working electrodes, respectively. The system was run on a PC through GPES 4.9 software.

In order to obtain information about the morphology and size of the electrodeposited gold nanostructures, field emission scanning electron microscopy (FESEM) was performed by the instrument Zeiss, Sigma-IGMA/VP (Germany).

Procedures

In order to synthesize different gold nanostructures, electrodeposition method at various experimental conditions was employed. To this purpose, potentiostatic electrodeposition was performed from an $AuCl_4^-$-containing solution. Different supporting electrolytes and different additives were added to this solution (the synthesis solution). The color of the synthesis solutions was all bright yellow. In some procedures, ultrasound wave of 45-W power was irradiated to the synthesis solution and also the Au electrode surface. Before electrodeposition, the Au electrode was polished by sand papers and then on a polishing pad with 50-nm alumina powder lubricated by glycerin. Polishing was continued to attain a mirror-like surface. The electrode was then cleaned by immersion in a 1:3 water/ethanol mixture and ultrasonication for 5 min in an ultrasound bath. The electrode was further electropolished by immersion in a 0.5-mol L^{-1} H_2SO_4 solution and applying potential in the range of cathodic and anodic edges of the electrolyte stability in a regime of cyclic voltammetry for 25 consecutive cycles. Upon this pretreatment, clean and stable Au electrode surface was attained. The Au electrode was then placed in the cell containing the synthesis solutions. Electrodeposition was done at desired potentials and times. The nanostructures gold electrodeposited-Au electrodes were then rinsed thoroughly with distilled water.

Electrochemical measurements to obtain the real surface area and calculation of roughness factor for the electrodeposited surface were performed as follows. After electrodeposition of gold nanostructures, the electrode was transferred to a solution of KCl (0.5 mol L^{-1}) containing $K_4Fe(CN)_6$ (0.5 mmol L^{-1}) as a redox probe and cyclic voltammograms at different potential sweep rates were recorded. The real surface areas were obtained from the Randles-Sevcik equation [44] and the value of 7.60×10^{-6} cm s^{-1} for the diffusion coefficient of $Fe(CN)_6^{4-}$ [45].

Results

The first gold nanostructure was electrodeposited on the Au electrode surface in the presence of arginine (20 mmol L^{-1} $HAuCl_4$ + 0.5 mol L^{-1} H_2SO_4 + 150 mmol L^{-1} arginine), at 0 V, and the electrodeposition duration was 600 s (Au/nano-Au-Arg). Figure 1a shows FESEM images of Au/nano-Au-Arg electrode surface with different magnifications. At the low magnification, spear-like gold nanostructures with small sawteeth are observed. Higher magnification images show that these nanospears comprised nanowedges of 150–300 nm mean length with sawtooth-shaped surfaces. When electrodeposition was performed in the presence of aspartic acid (20 mmol L^{-1} $HAuCl_4$ + 0.5 mol L^{-1} H_2SO_4 + 150 mmol L^{-1} aspartic acid) at 0 V for 600 s (Au/nano-Au-Asp), gold was electrodeposited as spherical and highly smooth surface nanoparticles with a mean diameter of 162 ± 5 nm. FESEM images of Au/nano-Au-Asp are shown in Fig. 1b.

Electrodeposition of gold nanostructure in the presence of histidine (20 mmol L^{-1} $HAuCl_4$ + 0.5 mol L^{-1} H_2SO_4 + 150 mmol L^{-1} histidine) at 0 V for 600 s (Au/nano-Au-Hist) resulted in the morphology of dendrite with different sizes of hyperbranched pine-like structures (Fig. 2). The dendrites, however, comprise the building units of about 150- to 200-nm nanoparticles. Therefore, the dendritic nanostructure electrodeposited in the presence of histidine has a hierarchical structure.

Electrodeposition of gold in the presence of lysine (20 mmol L^{-1} $HAuCl_4$ + 0.5 mol L^{-1} H_2SO_4 + 150 mmol L^{-1} lysine) at the potential of 0 V for 600 s (Au/nano-Au-Lys) formed long dendrites; each dendrite is also hierarchical nanostructure consisting of an array of parallel arranged pyramidal nanoparticles (Fig. 3).

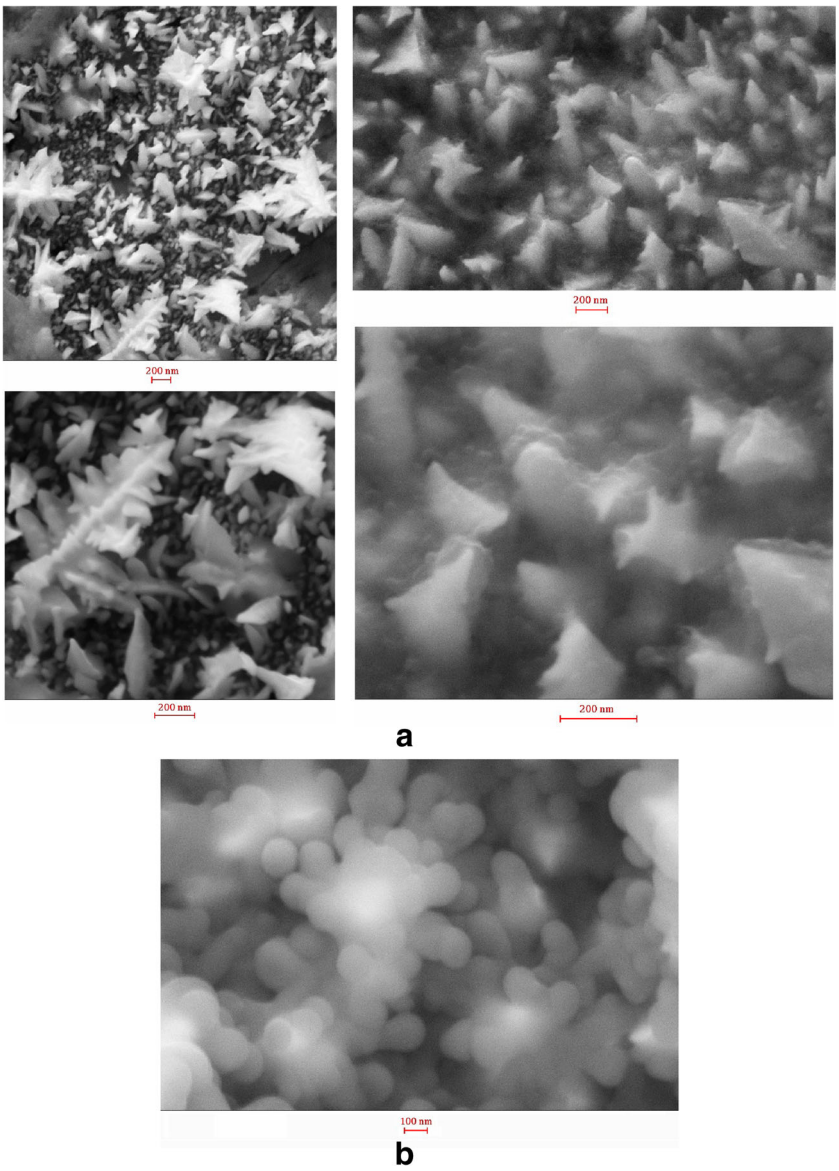

Fig. 1 **a** FESEM images of Au/nano-Au-Arg electrode surface with different magnifications. The electrodeposition solution contained 20 mmol L^{-1} $HAuCl_4$ + 0.5 mol L^{-1} H_2SO_4 + 150 mmol L^{-1} arginine. The electrodeposition potential was 0 V, and the electrodeposition duration was 600 s. **b** A FESEM image of Au/nano-Au-Asp electrode surface. The electrodeposition solution contained 20 mmol L^{-1} $HAuCl_4$ + 0.5 mol L^{-1} H_2SO_4 + 150 mmol L^{-1} aspartic acid. The electrodeposition potential was 0 V, and the electrodeposition duration was 600 s

Electrodeposition in the presence of glucosamine (20 mmol L^{-1} $HAuCl_4$ + 0.5 mol L^{-1} H_2SO_4 + 150 mmol L^{-1} glucosamine) at 0 V with an electrodeposition time of 600 s (Au/nano-Au-Glua) resulted in the formation of nanoparticles with different shapes and sizes. A FESEM image of the Au/nano-Au-Glua electrode is presented in Fig. 4.

Electrodeposited gold structure without using amino compounds in the presence of PVP (5 mmol L^{-1} $HAuCl_4$ + 0.5 mol L^{-1} H_2SO_4 + 1.0 g L^{-1} PVP, average molecular weight of 40,000) at 300 mV with an electrodeposition time of 500 s (Au/nano-Au-PVP) was nanocubes with a mean length of 104 ± 4 nm (Fig. 5).

If no additive was employed in the electrodeposition solution (5 mmol L^{-1} $HAuCl_4$ + 0.5 mol L^{-1} KCl) at 300 mV for 500 s (Au/nano-Au), the resultant nanostructure obtained in these conditions was oblong-shaped and polyangular rods. Figure 6 shows FESEM images of the Au/nano-Au electrode surface with two different magnifications. Each rod comprises two pyramids and appears as bipyramidal oblongs.

For sonoelectrodeposition of gold without any additive with a positive potential of 300 mV for 500 s, the synthesis solution (5 mmol L^{-1} $HAuCl_4$ + 0.5 mol L^{-1} KCl) and also the Au electrode surface were irradiated by ultrasound wave (Au/nano-Au-us3). The morphology of Au/nano-Au-us3 is similar to that of Au/nano-Au (Fig. 7a). The results indicate that the ultrasound irradiation of the synthesis solution and the depositing surface did not affect the morphology of the surface. On the other hand, sonoelectrodeposition without any additive (5 mmol L^{-1} $HAuCl_4$ + 0.5 mol L^{-1} KCl) at a highly negative potential

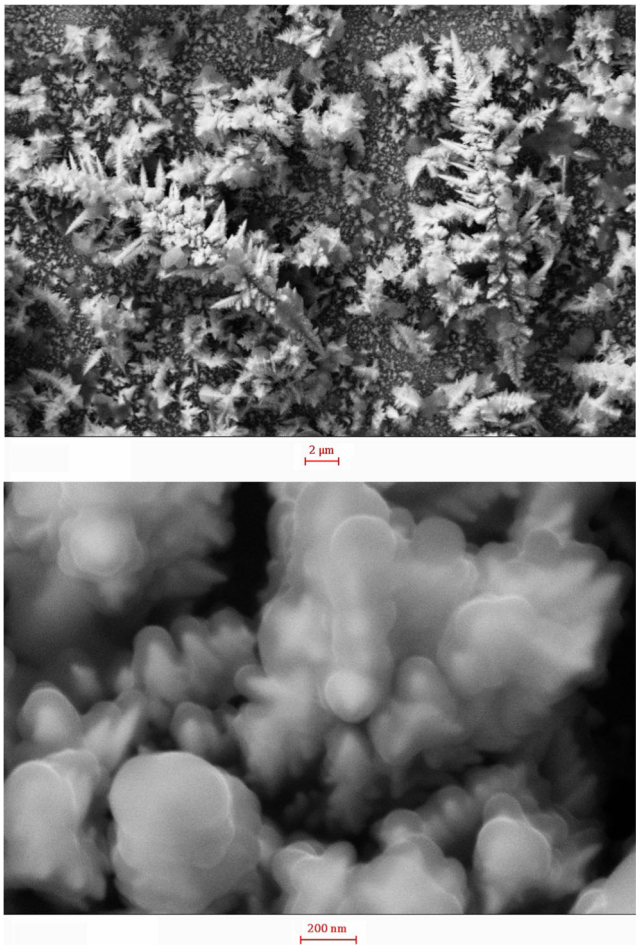

Fig. 2 FESEM images of Au/nano-Au-Hist electrode surface with different magnifications. The electrodeposition solution contained 20 mmol L^{-1} $HAuCl_4$ + 0.5 mol L^{-1} H_2SO_4 + 150 mmol L^{-1} histidine. The electrodeposition potential was 0 V, and the electrodeposition duration was 600 s

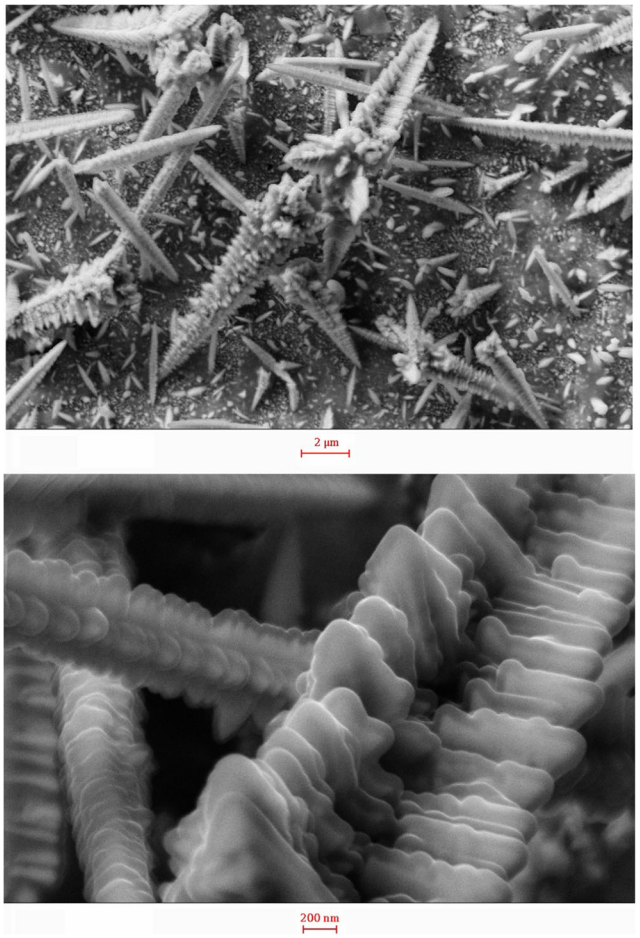

Fig. 3 FESEM images of Au/nano-Au-Lys electrode surface with different magnifications. The electrodeposition solution contained 20 mmol L^{-1} $HAuCl_4$ + 0.5 mol L^{-1} H_2SO_4 + 150 mmol L^{-1} lysine. The electrodeposition potential was 0 V, and the electrodeposition duration was 600 s

of −1800 mV for 300 s while the synthesis solution and also the Au electrode surface were irradiated by ultrasound wave was performed (Au/nano-Au-us18). Figure 7b shows FESEM images of Au/nano-Au-us18 with different magnifications. The nanostructure has a complex morphology and at low magnification comprises clung ribbons which are partly covered by blooms. At higher magnifications, FESEM images show nanoparticles of gold deposited on the connected smooth surface nanoribbons.

Real surface areas of the synthesized gold nanostructures were electrochemically determined using the redox probe of ferrocyanide. Cyclic voltammograms of $Fe(CN)_6^{4-}$ recorded at different potential sweep rates using the gold-electrodeposited Au electrodes (Supplementary materials) and the real surface area of the nanostructures were determined, as reported in Table 1. Electrochemical activity of the synthesized gold nanostructures was evaluated in the course of electrooxidation/electroreduction

Fig. 4 A FESEM image of Au/nano-Au-Glua electrode surface. The electrodeposition solution contained 20 mmol L^{-1} $HAuCl_4$ + 0.5 mol L^{-1} H_2SO_4 + 150 mmol L^{-1} glucosamine. The electrodeposition potential was 0 V, and the electrodeposition duration was 600 s

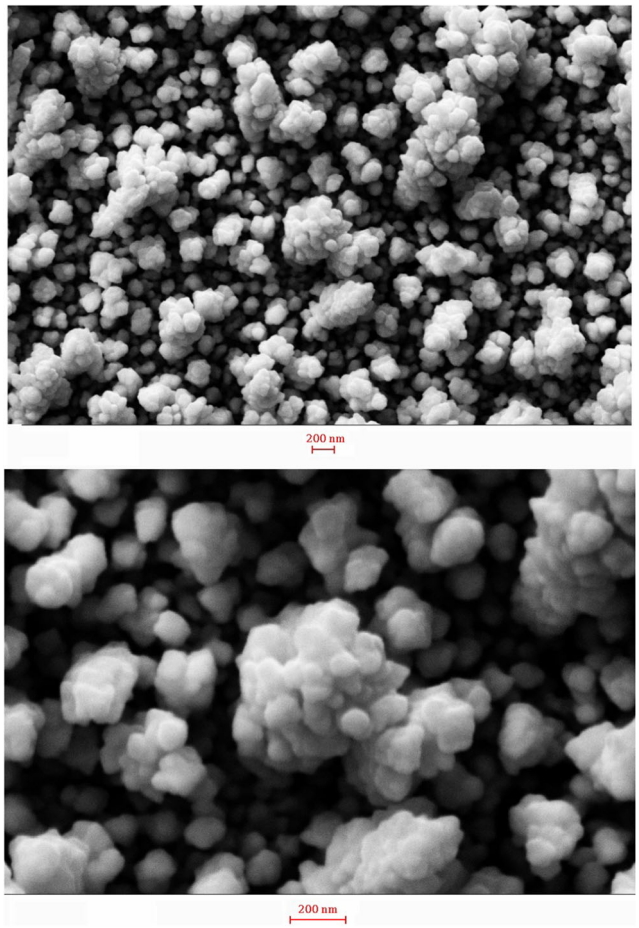

Fig. 5 FESEM images of Au/nano-Au-PVP electrode surface with different magnifications. The electrodeposition solution contained 5 mmol L^{-1} $HAuCl_4$ + 0.5 mol L^{-1} H_2SO_4 + 1.0 g L^{-1} PVP. The electrodeposition potential was 300 mV, and the electrodeposition duration was 500 s

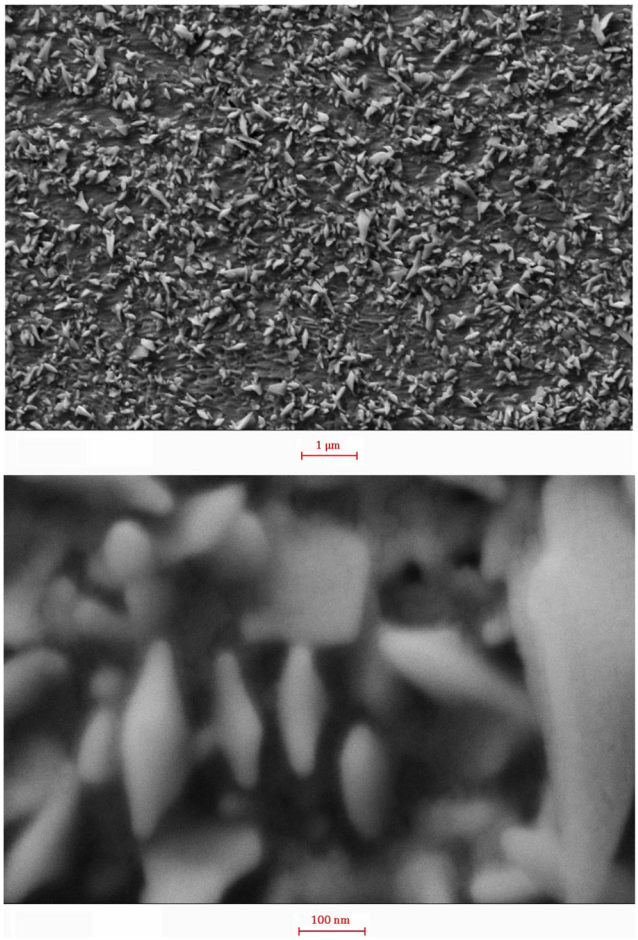

Fig. 6 FESEM images of Au/nano-Au electrode surface with different magnifications. The electrodeposition solution contained 5 mmol L^{-1} $HAuCl_4$ + 0.5 mol L^{-1} KCl. The electrodeposition potential was 300 mV, and the electrodeposition duration was 500 s

of some biologically important compounds of ascorbic acid, glucose, and hydrogen peroxide (Supplementary materials). The gold nanostructures represented different activities toward different compounds (Table 1).

Discussion

Affinity of amino acid to bind with gold surface has been investigated both theoretically [46–49] and experimentally [48, 50, 51]. Amino acids have also been employed as soft templates for the synthesis of gold nanostructures [52]. Gold has also affinity to amine functional group [48, 51, 53, 54]. During the electrodeposition of gold, nucleation, adsorption (of additives), branching, and growth are the dominant steps. From these steps, kinetics of the growth step is slow and controls the total process [55]. At the early stage of the electrodeposition, $AuCl4^-$ was quickly reduced to gold atoms, followed by distribution of gold nuclei at the surface. If an additive (amino acids, glucosamine, or PVP) is present in the solution, it is rapidly and selectively adsorbed (mainly via amine groups) on the specific planes of gold crystal. This adsorption prevents the newly generated gold atoms to be aggregated with the previously deposited ones. On the other hand, the additives act as shape-directing agents and depending on their chemical structures facilitate the gold crystal growth at a specific direction(s). If the electrodeposition is performed at highly negative potentials, the hydrogen co-evolution process would be the main shape-directing agent.

Regarding the real surface areas, gold nanospears with small sawteeth had the highest and gold pine-like hyperbranched nanodendrites and gold nanoparticles had the lowest real surface areas. There was a wide range of roughness factor, and different shapes of gold provide huge different surface areas. Electrochemical activity of the gold structures was also different depending on the shape and size from both

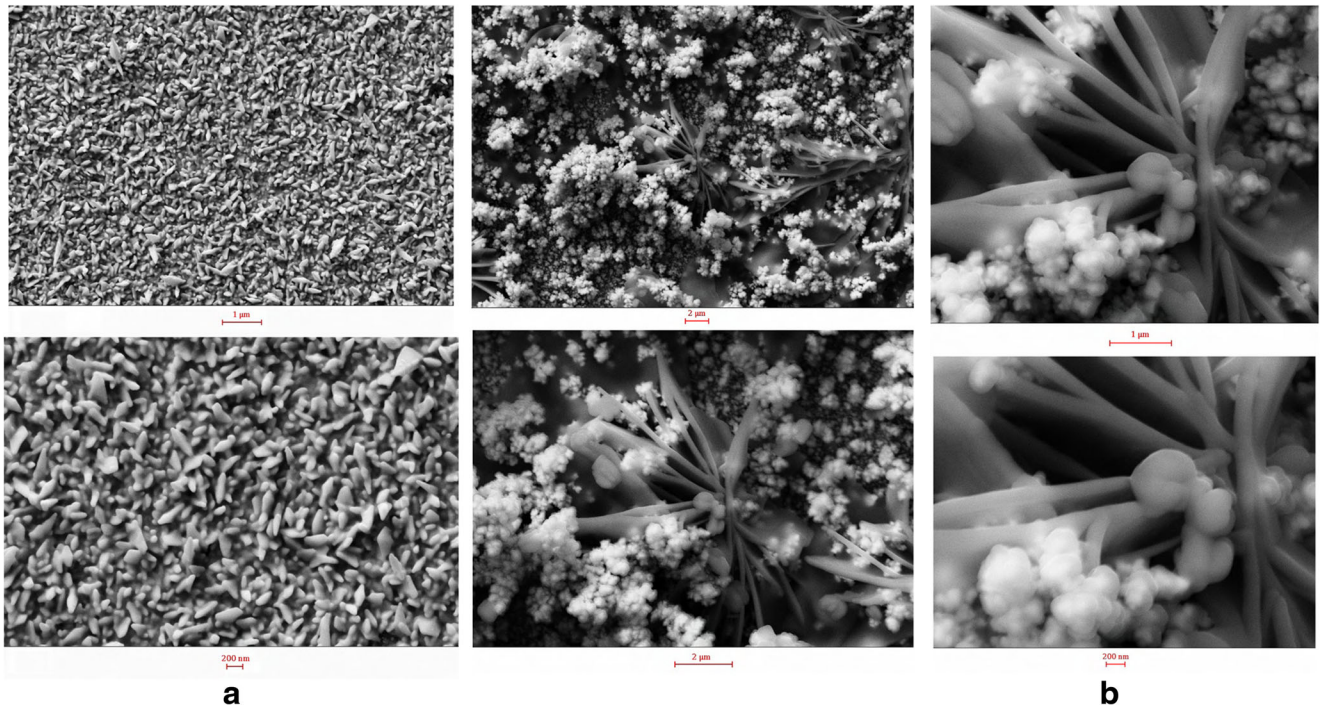

Fig. 7 **a** FESEM images of Au/nano-Au-us3 electrode surface with different magnifications. The electrodeposition solution contained 5 mmol L^{-1} $HAuCl_4$ + 0.5 mol L^{-1} KCl. The electrodeposition potential was 300 mV, and the electrodeposition duration was 500 s. The synthesis solution and also the Au electrode surface were irradiated by ultrasound wave. **b** FESEM images of Au/nano-Au-us18 with different magnifications. The electrodeposition solution contained 5 mmol L^{-1} $HAuCl_4$ + 0.5 mol L^{-1} KCl. The electrodeposition potential was −1800 mV, and the electrodeposition duration was 300 s. The synthesis solution and also the Au electrode surface were irradiated by ultrasound wave

kinetic and thermodynamic points of view. The different peak currents for the electroreduction/electrooxidation of the analytes can be related to the active surface areas of the gold nanostructures and different shapes and sizes causing the reactions to occur at different potentials. It depended on both the entity of the analyte and the shape and size of the gold nanostructures; the best gold nanostructure can be selected for a special analyte to electroreduce/electrooxidize.

Table 1 Characteristics of different synthesized gold nanostructures

Electrode	Shape of nanostructure	Area	RF	AA-E_p	AA-i_p	GL-E_p	GL-i_p	H_2O_2-E_p	H_2O_2-i_p
Au/nano-Au-Arg	Nanospears with small sawteeth	0.99	31.4	21	4.9	362	37.9	−522	4.45
Au/nano-Au-Asp	Highly smooth surface nanoparticles	0.72	23.0	209	8.1	384	12.1	−679	7.12
Au/nano-Au-Hist	Pine-like hyperbranched nanodendrites	0.26	8.2	43	22.4	293	15.8	−561	23.23
Au/nano-Au-Lys	Hierarchical nanodendrites	0.84	26.9	68	5.4	288	0.42	−548	6.12
Au/nano-Au-Glua	Nanoparticles	0.26	8.2	59	19.5	301	0.81	−489	18.81
Au/nano-Au-PVP	Nanocubes	0.48	15.2	238	10.5	357	6.9	−615	8.96
Au/nano-Au	Bipyramidal and polyangular nanorods	0.56	17.7	436	9.2	342	0.13	−763	10.54
Au/nano-Au-us3	Bipyramidal and polyangular nanorods	0.59	18.8	100	6.6	392	3.2	−648	8.81
Au/nano-Au-us18	Nanoribbons covered by blooms	0.73	23.2	15	7.6	374	67.1	−161	7.49

All the peak currents were measured at the potential sweep rate of 50 mV s^{-1}. The geometric surface area of the electrode was 0.031 cm^2

Area real surface area (cm^2), *RF* roughness factor, *AA-E_p* ascorbic acid electrooxidation peak potential (mV), *AA-i_p* ascorbic acid electrooxidation peak current density (μA cm^{-2}; the current density was obtained with respect to the real surface area), *GL-E_p* glucose electrooxidation peak potential in the forward scan in the voltammograms (mV, glucose produced anodic peaks in both the forward and reverses scans in the voltammograms), *GL-i_p* glucose electrooxidation peak current density in the forward scan in the voltammogram (μA cm^{-2}), *H_2O_2-E_p* hydrogen peroxide electroreduction peak potential (mV), *H_2O_2-i_p* hydrogen peroxide electroreduction peak current density (μA cm^{-2}; the current density was obtained with respect to the real surface area)

Conclusion

This study showed that electrodeposition method can provide a variety of gold nanostructures with diverse size, shape, and electrochemical activity. The green additives, dc potential, and ultrasound irradiation played the major roles in the fabrication of these nanostructures. The surface of the nanostructures had different roughness and electrochemical activities related to the size and shape. The method can be extendable to the synthesis of other gold nanostructures and similar noble metal nanostructures.

Acknowledgments We would like to thank the Research Council of Shiraz University of Medical Sciences (7919) for supporting this research.

References

1. Daniel MC, Astruc D (2004) Gold nanoparticles: assembly, supramolecular chemistry, quantum size related properties, and applications toward biology, catalysis, and nanotechnology. Chem Rev 104:293–346
2. Kim F, Song H, Yang P (2002) Photochemical synthesis of gold nanorods. J Am Chem Soc 124:14316–14317
3. Hutchinson YO, Liu YP, Kiely C, Kiely CJ, Brust M (2001) Templated gold nanowire self-assembly on carbon substrates. Adv Mater 13:1800–1803
4. Gopal J, Hasan N, Manikandan M, Wu HF (2013) Bacterial toxicity/compatibility of platinum nanospheres, nanocuboids and nanoflowers. Sci Rep 3:1260
5. Sun Y, Xia Y (2003) Triangular nanoplates of silver: synthesis, characterization, and use as sacrificial templates for generating triangular nanorings of gold. Adv Mater 15:695–699
6. Zhan J, Du J, Han B, Liu Z, Jiang T, Zhang Z (2006) Sonochemical formation of single-crystalline gold nanobelts. Angew Chem 45: 1116–1119
7. Sun Y, Xia Y (2002) Shape-controlled synthesis of gold and silver nanoparticles. Science 298:2176–2179
8. Shankar SS, Rai A, Ankamwar B, Singh A, Ahmad A, Sastry M (2004) Biological synthesis of triangular gold nanoprisms. Nat Mater 3:482–488
9. Sun X, Dong S, Wang E (2004) Large-scale synthesis of micrometer scale single crystalline Au plates of nanometer thickness by a wet-chemical route. Angew Chem 43:6360–6363
10. Tian T, Tatsuma T (2004) Plasmon-induced photoelectrochemistry at metal nanoparticles supported on nanoporous TiO2. Chem Commun 1810–1811
11. Lopez-Acevedo O (2010) Chirality and electronic structure of the thiolate-protected Au38 cluster. J Am Chem Soc 132:8210–8218
12. Burda C, Chen X, Narayanan R, El-Sayed MA (2005) Chemistry and properties of nanocrystals of different shapes. Chem Rev 105: 1025–1102
13. Lagos MJ, Sato F, Autreto PAS, Galvao DS, Rodrigues V, Ugarte D (2010) Temperature effects on the atomic arrangement and conductance of atomic-size gold nanowires generated by mechanical stretching. Nanotechnology 21:485702
14. Song Y, Murray RW (2002) Dynamics and extent of ligand exchange depend on electronic charge of metal nanoparticles. J Am Chem Soc 124:7096–7102
15. Miller MM, Lazarides AA (2005) Sensitivity of metal nanoparticle surface plasmon resonance to the dielectric environment. J Phys Chem B 109:21556–21565
16. Sardar R, Funston AM, Mulvaney P, Murray RW (2009) Gold nanoparticles: past, present, and future. Langmuir 25:13840–13851
17. Hammer B (2006) Special sites at noble and late transition metal catalysts. Top Catal 37:3–16
18. Liu Z, Searson PC (2006) Single nanoporous gold nanowire sensors. J Phys Chem B 110:4318–4322
19. Major TA, Devadas M, Lo SS, Hartland GV (2013) Optical and dynamical properties of chemically synthesized gold nanoplates. J Phys Chem C 117:1447–1452
20. Shin HS, Hong JY, Huh S (2013) 2-Thiopheneacetic acid directed synthesis of Au nanorosette as an SERS-active substrate. ACS Appl Mater Interfaces 5:1429–1435
21. Zhang GM (2013) Functional gold nanoparticles for sensing applications. Nanotechnol Rev 2:269–288
22. Debe MK (2012) Electrocatalyst approaches and challenges for automotive fuel cells. Nature 486:43–51
23. Huang X, Jain PK, El-Sayed IH, El-Sayed MA (2007) Plasmonic photothermal therapy (PPTT) using gold nanoparticles. Lasers Med Sci 23:217–228
24. Hajipour MJ, Fromm KM, Ashkarran AA, Aberasturi DJ, Larramendi IR, Rojo T, Serpooshan V, Parak WJ, Mahmoudi M (2012) Antibacterial properties of nanoparticles. Trends Biotechnol 30:499–511
25. Muscarella M, Pathak YV (2012) Targeted nanoparticles in radiotherapy in: antibody-mediated drug delivery systems: concepts, technology, and applications. John Wiley and Sons, New York
26. Komsiyska L, Staikov G (2008) Electrocrystallization of Au nanoparticles on glassy carbon from HClO4 solution containing [AuCl4]. Electrochim Acta 54:168–172
27. Sattarahmady N, Tondro GH, Golchin M, Heli H (2015) Gold nanoparticles biosensor of Brucella spp. genomic DNA: visual and spectrophotometric detections. Biochem Eng J 97:1–7
28. Sattarahmady N, Movahedpour A, Heli H, Hatamd GR (2016) Gold nanoparticles-based biosensing of Leishmania major kDNA genome: visual and spectrophotometric detections. Sens Actuat B 235:723–731
29. Zhai C, Sun X, Zhao W, Gong Z, Wang X (2013) Acetylcholinesterase biosensor based on chitosan/prussian blue/multiwall carbon nanotubes/hollow gold nanospheres nanocomposite film by one-step electrodeposition. Biosens Bioelectron 42:124–130
30. Rahi A, Sattarahmady N, Dehdari Vais R, Heli H (2015) Sonoelectrodeposition of gold nanorods at a gold surface—application for electrocatalytic reduction and determination of nitrofurazone. Sens. Actuat. B 210:96–102
31. Heli H, Rahi A (2016) Synthesis and applications of nanoflowers. Recent Pat Nanotechnol 10:86–115
32. Dehdari Vais R, Sattarahmady N, Karimian K, Heli H (2015) Green electrodeposition of gold hierarchical dendrites of pyramidal nanoparticles and determination of azathioprine. Sens Actuat B 215:113–118
33. Song JH, Fan SJ, Yu JY, Ye KH, Xu CW (2012) In situ synthesis of metal nanoparticles on single-layer graphene oxide and reduced graphene oxide surfaces. Int J Electrochem Sci 7:10842–10850
34. Montes MO, Mayoral A, Deepak FL, Parsons JG, Jose-Yacaman M, Peralta-Videa JR, Gardea-Torresdey JL (2011) Anisotropic gold nanoparticles and gold plates biosynthesis using alfalfa extract. J Nanopart Res 13:3113–3121
35. Tin Y, Lui H, Zhao G, Tatsuma T (2006) Shape-controlled electrodeposition of gold nanostructures. J Phys Chem B 110:23478–23481
36. Heli H, Amirizadeh O (2016) Non-enzymatic glucose biosensor based on hyperbranched pine-like gold nanostructure. Mater Sci Eng C 63:150–154

37. Rahi A, Sattarahmady N, Heli H (2015) Zepto-molar electrochemical detection of Brucella genome based on gold nanoribbons covered by gold nanoblooms. Sci Rep 5:Article number 18060
38. Rahi A, Sattarahmady N, Heli H (2016) Label-free electrochemical aptasensing of the human prostate-specific antigen using gold nanospears. Talanta 156-157:218–224
39. Moradi M, Sattarahmady N, Rahi A, Hatam GR, Rezayat Sorkhabadi SM, Heli H (2016) A label-free, PCR-free and signal-on electrochemical DNA biosensor for Leishmania major based on gold nanoleaves. Talanta 161:48–53
40. Moradi M, Sattarahmady HGR, Heli H (2016) Electrochemical genosensing of Leishmania major using gold hierarchical nanoleaflets. J Biol Today's World 5:128–136
41. Morasso C, Mayoral A, Deepak FL, Parsons M, Jose-Yacaman M, Peralta-Videa JR, Gardea-Torresdey JL (2014) One-step synthesis of star-like gold nanoparticles for surface enhanced Raman spectroscopy. Mater Chem Phys 143:1215–1221
42. Feng JJ, Lv ZY, Qin SF, Li AQ, Fei Y, Wang AJ (2013) N-methylimidazole-assisted electrodeposition of Au porous textile-like sheet arrays and its application to electrocatalysis. Electrochim Acta 102:312–318
43. Rahi A, Sattarahmady N, Heli H (2016) An ultrasensitive electrochemical genosensor for Brucella based on palladium nanoparticles. Anal Biochem 510:11–17
44. Bard AJ, Faulkner LR (2001) Electrochemical methods. John Wiley, New York
45. Wang SF, Xu Q (2007) Electrochemical parameters of ethamsylate at multi-walled carbon nanotube modified glassy carbon electrodes. Bioelectrochem 70:296–300
46. Hoefling M, Iori F, Corni S, Gottschalk KE (2010) Interaction of amino acids with the Au(111) surface: adsorption free energies from molecular dynamics simulations. Langmuir 26:8347–8351
47. Ramezani F, Amanlou M, Rafii-Tabar H (2014) Comparison of amino acids interaction with gold nanoparticle. Amino Acids 46: 911–920
48. Crespilho FN, Lima FCA, da Silva ABF, Oliveira ON, Zucolotto V (2009) The origin of the molecular interaction between amino acids and gold nanoparticles: a theoretical and experimental investigation. Chem Phys Lett 469:186–190
49. Feng J, Pandey RB, Berry RJ, Farmer BL, Naik RR, Heinz H (2011) Adsorption mechanism of single amino acid and surfactant molecules to Au {111} surfaces in aqueous solution: design rules for metal-binding molecules. Soft Matter 7:2113–2120
50. Sethi M, Knecht MR (2009) Experimental studies on the interactions between Au nanoparticles and amino acids: bio-based formation of branched linear chains. ACS Appl Mater Interfaces 1:1270–1278
51. Joshi H, Shirude PS, Bansal V, Ganesh KN, Sastry M (2004) Isothermal titration calorimetry studies on the binding of amino acids to gold nanoparticles. J Phys Chem B 108:11535–11540
52. Maruyama T, Fujimoto Y, Maekawa T (2015) Synthesis of gold nanoparticles using various amino acids. J Colloid Interface Sci 447:254–257
53. Wright LB, Merrill NA, Knecht MR, Walsh TR (2014) Structure of arginine overlayers at the aqueous gold interface: implications for nanoparticle assembly. ACS Appl Mater Interfaces 6:10524–10533
54. Lv ZY, Li AQ, Fei Y, Li Z, Chen JR, Wang AJ, Feng JJ (2013) Facile and controlled electrochemical route to three-dimensional hierarchical dendritic gold nanostructures. Electrochim Acta 109: 136–144
55. You H, Yang S, Ding B, Yang H (2013) Synthesis of colloidal metal and metal alloy nanoparticles for electrochemical energy applications. Chem Soc Rev 42:2880–2904